Seafloor Control on Sea Ice

S. V. Nghiem[a], P. Clemente-Colón[b], I. G. Rigor[c], D. K. Hall[d], and G. Neumann[a]

[a]Jet Propulsion Laboratory, California Institute of Technology, Pasadena, CA 91109, USA

[b]National/Naval Ice Center, 4251 Suitland Road, Washington, DC 20395, USA

[c]Applied Physics Laboratory, University of Washington, Seattle, WA 98105, USA

[d]NASA Goddard Space Flight Center, Greenbelt, MD 20771, USA

Abstract

The seafloor has a profound role in Arctic sea ice formation and seasonal evolution. Ocean bathymetry controls the distribution and mixing of warm and cold waters, which may originate from different sources, thereby dictating the pattern of sea ice on the ocean surface. Sea ice dynamics, forced by surface winds, are also guided by seafloor features in preferential directions. Here, satellite mapping of sea ice together with buoy measurements are used to reveal the bathymetric control on sea ice growth and dynamics. Bathymetric effects on sea ice formation are clearly observed in the conformation between sea ice patterns and bathymetric characteristics in the peripheral seas. Beyond local features, bathymetric control appears over extensive ice-prone regions across the Arctic Ocean. The large-scale conformation between bathymetry and patterns of different synoptic sea ice classes, including seasonal and perennial sea ice, is identified. An implication of the bathymetric influence is that the maximum extent of the total sea ice cover is relatively stable, as observed by scatterometer data in the decade of the 2000s, while the minimum ice extent has decreased drastically. Because of the geologic control, the sea

ice cover can expand only as far as it reaches the seashore, the continental shelf break, or other pronounced bathymetric features in the peripheral seas. Since the seafloor does not change significantly for decades or centuries, sea ice patterns can be recurrent around certain bathymetric features, which, once identified, may help improve short-term forecast and seasonal outlook of the sea ice cover. Moreover, the seafloor can indirectly influence cloud cover by its control on sea ice distribution, which differentially modulates the latent heat flux through ice covered and open water areas.

1. Introduction

In the Arctic, the minimum sea ice extent (SIE) in the summer-fall transition has undergone drastic reduction, far exceeding the worst-case projections from climate models of the Intergovernmental Panel on Climate Change Fourth Assessment Report (Stroeve et al, 2007; Allison et al., 2009). However, the maximum SIE in the winter-spring transition period has been much more stable in the past decade (Nghiem et al., 2008). Table 1 shows a small decreasing trend in the maximum SIE that is insignificant compared to the much more severe reduction trend in the minimum SIE in the decade of 2000s as observed by the QuikSCAT (QS) satellite scatterometer. The comparable results between maximum SIE and March-average SIE (Table 1) indicate the persistence of the maximum SIE.

While the large reduction in summer SIE has been primarily associated with climate change (e.g., Richardson et al., 2009), the stability or small change in the maximum SIE suggests some significant influences by geological factors such as the seafloor, which largely remains invariant in the decadal time scale. Effects of seafloor features on sea ice patterns have been reported in

several local areas in the Arctic peripheral seas. In the Barents Sea, a sea ice barrier forms along a deep channel from the Franz Josef-Victoria trough to the Hinlopen Basin while the Bear Island ice tongue forms on the shallow bathymetry (Nghiem et al., 2005). Thus, sea ice can grow and reside preferentially on either deep or shallow bathymetry depending on how warm and cold waters are guided by the seafloor.

In the Greenland Sea, the Odden ice tongue protrudes as far as 5^{o} eastward from the main ice pack between 73^{o} and 77^{o} N where ocean currents, deep convection, and bathymetry may have a role (Bourke et al., 1992; Shuchman et al., 1998; Comiso et al., 2001). In the Chukchi Sea, a Taylor column over the Herald Shoal traps cold water and sea ice persists over the shoal as the general ice cover recedes (Martin and Drucker, 1997). Along the north Alaskan coast across the Chukchi Sea and the Beaufort Sea, observations with the RADARSAT Synthetic Aperture Radar (SAR) imagery revealed that isobaths near 18-m depth are a good approximation for landfast ice extent, which has shown no significant difference between recent years and the 1970s (Mahoney et al., 2007).

In this paper, we use sea ice results from QS observations together with bathymetric data to investigate the influence of the seafloor on Arctic sea ice formation and seasonal evolution. The analysis includes local bathymetric features in the peripheral seas as well as regional seafloor characteristics across the Arctic Ocean. Results are used to explain the relative stability of the maximum SIE in the decade of 2000s and to discuss the potential use of bathymetry in sea ice forecasts and seasonal outlooks. After describing the approach in Section 2, results and discussions are presented in Section 3, and the summary and concluding remarks are given in the last section.

Parameter	Rate of change million km^2/year	Correlation coefficient	Standard deviation million km^2
Minimum SIE (in summer-fall)	−0.204 (−3.5 %)	−0.824	0.307 (5.2 %)
Maximum SIE (in winter-spring)	−0.081 (−0.6 %)	−0.601	0.404 (2.8 %)
Average SIE (in March)	−0.062 (−0.4 %)	−0.521	0.291 (2.0 %)

Table 1. Change of sea ice extent (SIE) in the decade of 2000s (2000-2009) observed by the QuikSCAT satellite scatterometer. The minimum values of SIE were in summer-fall, the maximum were in winter-spring, and the averages were calculated with available data from all days in March for each year. The percentage values in parentheses are computed with the decadal mean values of minimum, maximum, and average SIE, respectively.

2. Approach

Bathymetric data and sea ice measurements are compared to identify the conformation between patterns of the seafloor characteristics and sea ice distribution. For bathymetry, the International Bathymetric Chart of the Arctic Ocean (IBCAO) is used in this paper. IBCAO consists of bathymetric data north of 64^o N with a grid spacing of 2.5 km (Jakobsson et al., 2000) and an improved version for a 2-km grid (Jakobsson et al., 2008). Because of the geographic limit at 64^o N, some regions of the Arctic peripheral seas are not included in IBCAO such as the southern extent of the Bering Sea, where bathymetric data are necessary for the analysis together with sea ice measurements. To complement IBCAO, ETOPO5 data are used. ETOPO5 (National Geophysical Data Center, 1988) is a digital database of both land and seafloor elevations of the Earth on a 5-minute grid in latitude and longitude.

QS was launched in June 1999 and collected global backscatter data at the Ku-band frequency of 13.4 GHz (Tsai et al., 2000). With a large swath of 1400 km for the horizontal polarization and 1800 km for the vertical polarization, QS data covered the Arctic twice a day until a malfunction of the antenna rotary joint occurred in November 2009 (Nghiem et al., 2011). Arctic sea ice is identified from open water using QS backscatter measurements with a quadruplet algorithm, which is robust across a wide range of wind speed and wind directions (Nghiem et al., 2005). Once the ice cover is delineated, sea ice is classified into major ice classes including seasonal (first-year) ice, perennial (multi-year) ice, and mixed ice based on distinctive signatures of the different ice classes at Ku band (Nghiem et al., 2006; Nghiem and Neumann, 2007). Sea ice results are posted in a regular grid at 0.25^{o} in latitude and in longitude. Since QS, IBCAO, and ETOPO5 have different grid spacings, the 5-minute grid is selected as the common one to resample all data into every 5-minute or 1/12-degree pixel.

The comparison between sea ice and bathymetry patterns is characterized in two different analyses. First, in a statistical analysis, the histogram of number of sea ice parcels is obtained as a function of the ocean depth from bathymetry data. The histogram represents the distribution function of cumulative sea ice, in percentage, at different ocean depths. Second, in a minimization analysis, the deviation D_j is calculated for each set of the closest distance from each point on the edge of the extent of a sea ice class to each isobath marked with index j within the range of j=1 to j=M. The closest isobath with deviation D_B is determined as the minimum average distance from all D_j values as $D_B = \min\{D_j, j \in [1, M]\}$, which is best conformed to the sea ice edge.

3. Results

3.1. Bering Sea

The seasonal advance and retreat of the sea ice edge is strongly influenced by dynamic and thermodynamic effects indicating a close interplay of the atmosphere, sea ice, and ocean. Air-ice-ocean interactions were observed in the Bering, Chukchi, Beaufort, and East Siberian Seas where both sea ice and wind vectors over open water were measured contemporaneously by QS (Nghiem et al., 2006). An animation of the QS sea ice and wind results, published as auxiliary materials available in html for doi:10.1029/2006GL027198 and at the site http://ourocean.jpl.nasa.gov/beringsea.html (Nghiem et al., 2006), reveals how southerly and northerly winds drive the sea ice cover over a large area in a short time scale (day) across the Bering and Chukchi Seas, where the sea ice edge advances and retreats in phase with wind forcing in the fall to spring seasons.

Southerly winds can effectively force the ice retreat by: advecting warmer air northward and melting the ice from the surface, pushing the ice edge northward while compacting the ice cover farther to the north, and wind blowing across a large region of open water (a large fetch) and thus large waves with more effective mixing that bring up warmer water and melt the ice from below. In contrast, northerly winds can effectively force the ice to expand: advecting cold air from the north and freezing ocean water from the surface, pushing the ice edge southward while diverging the ice cover farther to the south, and wind blowing across a large region of sea ice without creating large waves (very small sea state in ice) while ice floes forced southward can suppress existing waves and effectively impede the water mixing and subsurface melt.

Northerly winds can advance the ice edge to the shelf break (e.g., observe ice cover change in the Bering Sea in March in http://ourocean.jpl.nasa.gov/beringsea.html), beyond which sea ice cannot effectively expand southward despite the consistency of the northerly winds. Warm water from the Alaskan Stream (Figure 1) leaks across deep passes in the Aleutian Chain as inflow into the deep basin of the Bering Sea (Stabeno and Reed, 1994) where the circulation of the Aleutian North Slope, Anadyr, and Kamchatka Currents is controlled by the regional bathymetry. Figure 1 illustrates an alignment of sea ice edge (3 March 2008) with the shelf-break bathymetry spanning over 1200 km across the Bering Sea. The ice extent follows the shelf break limited by the warm Anadyr current guided along the shelf break. In the southeastern edge of the sea ice cover (area delimited by the white oval in Figure 1), sea ice growth is hindered by an intrusion of warm water allowed by the gentle gradual slope of the local bathymetry as opposed to the steep shelf break in other areas. As it becomes colder in later days, sea ice can cover the shallower area in the oval until it reaches to the extent above the deep bathymetry. The conformation of the sea ice edge to the shelf break in the Bering Sea recurs in other years as observed by QS.

Quantitatively, the histogram in Figure 2 presents the cumulative percentage of sea ice cover at different depths in the Bering Sea. From the histogram, less than 10% of sea ice was located over ocean areas deeper than 300 m as most of the ice cover was on the Bering continental shelf. In this case, the ice edge was in the vicinity of the shelf break with the best-conformed isobath of 1300 m determined from the minimization approach. There is a divergence between the ice edge and the 1300-m isobath toward the southeastern edge of the ice cover corresponding to the area where the bathymetry has a gradual slope rather than a steep break.

3.2. Chukchi and Beaufort Seas

Numerical calculations from the Regional Ocean Model System (ROMS) show an abrupt onset of wind-driven upwelling when the ice edge retreated beyond the shelf break in summer (Carmack and Chapman, 2003), suggesting dramatic impacts on shelf-basin exchange as the sea ice cover reduced northward across the shelf break. Upwelling of warm Chukchi Summer Water of a Pacific origin on the Canadian Shelf of the Beaufort Sea can enhance ice melt in summer and hinder ice growth in fall. Pacific water influx across the Bering Strait could significantly transport heat via the Herald Valley, Central Channel, and Barrow Canyon pathways into the Chukchi and Beaufort Seas where the extensive melt pattern of sea ice over the regional continental shelf was consistent with theses inflows in summer 2007 (Woodgate et al., 2009).

A numerical sea-ice-ocean model indicates that 80% of total heating was from ocean surface heat flux and the remaining from ocean lateral heat flux convergence in the Pacific Sector of the Arctic, where the model analysis shows the dominance of surface melt in the early summer and the bottom-melt dominance later due to ocean heat transport as atmospheric heating declines (Steele et al., 2010). Furthermore, as sea ice retreated across the shelf, the lower albedo of open water compared to that of sea ice cover can increase the insolation heat in the regional water as observed from satellite and field measurements (Perovich et al., 2007a). In particular, high values of heat input from solar energy absorbed in areas of open water are found in shelf waters of the Chukchi and Beaufort Seas (Perovich et al., 2007b).

In recent years, the summer minimum of sea ice has retreated northward across and off the continental shelf, which may emphasize the role of bathymetry role on the pattern of sea ice cover as suggested above. Here, QS sea ice maps and IBCAO bathymetry data are presented to

show the pattern change of sea ice in the summer and fall of 2009. In addition to the capability to identify and map various sea ice classes, QS can delineate areas where melt occurs on the sea ice surface (Nghiem and Neumann, 2007), and detect the timing of melt onset and freeze-up (Nghiem and Neumann, 2007; Perovich et al., 2007a). By 20 September 2009, melting on sea ice was mostly completed except for a small elongated area along the ice edge to the west of Banks Island (2a). As the season was transitioning from summer to fall, seasonal (first-year) sea ice started to form in the Canada Basin (Figure 3a). At that time, the southern edge of the ice pack, marked by the yellow curve in Figure 3a, already retreated off the continental shelf in the Chukchi Sea across the Beaufort Shelf to the Canadian Shelf. This excessive reduction of sea ice allowed the strong onset of warm water upwelling as suggested by Carmack and Chapman (2003).

By 20 October 2009, seasonal sea ice had covered most of the Canada Basin (Figure 3b) as the freeze-up process continued into the fall season. However, the southern ice edge, delineated by the green curve in Figure 3b, was still constrained off the shelf break and the water surface across the shallow shelves remained ice-free. In the one-month period from 20 September 2009, winds were persistently blowing from the east as indicated by reanalysis data from the National Centers for Environment Prediction **(**NCEP) (Kalnay et al., 1996). This prevailing easterly wind condition favored the upwelling of warm water that hindered the regional ice growth. During the prolonged warm period, having anice-free surface, the low albedo allowed additional absorption of solar radiation in the early fall; this further delayed sea ice growth.

Data from the Moderate Resolution Imaging Spectroradiometer (MODIS) MOD35 cloud product (Ackerman et al., 2008) show persistent cloud cover over this region between 20 September and 20 October 2009. This is because sea ice cover affects latent heat, and

subsequently the cloud cover pattern. Consequently, long-wave radiation emanating from the open water was trapped by the pervasive clouds above the open water region resulting in further warming, known as the 'blanket effect' (Nghiem, 1998; Perovich et al., 1999; Sturm et al., 2003). Thus, the shelf bathymetry exerts control on the warm-water distribution that impacts subsequent ice-albedo-radiation interactions, and effectively results in the conformation of the sea ice edge along the shelf break. In this case, ice in the Beaufort Sea preferentially forms over the deep bathymetry as opposed to the case of the Bering Sea where sea ice is more persistent over the shallow bathymetry albeit in different seasons.

Beyond its effects on the sea ice edge, the bathymetry can also constrain the location of the boundary between different sea ice classes. This is evident in Figure 3c (20 November 2009) where the boundary between the seasonal sea ice and the perennial and mixed ice, denoted here as L_S, stretches through an extensive length of 1670 km along the vicinity of the shelf break. As air temperature decreased significantly in late November, seasonal (first-year) sea ice formed over the shelf areas where the seawater surface had not frozen a month earlier as seen in Figure 3b. Sea ice from the previous year was persistent over the deep bathymetry in the Canada Basin, where it survived the summer melt and thus became perennial sea ice by definition (Armstrong et al., 1973; Nghiem et al., 2006).

The above results of the change in sea ice patterns from summer to fall are summarized in Figure 3d, where contours of the sea ice edge are overlain on the IBCAO bathymetry map. In summer 2009, sea ice retreated off the shelf break. Into the early fall season, warm water kept the shallow shelves ice-free. Later in the fall when the temperature was lower, young seasonal sea ice formed with the boundary to older ice located close to the shelf break along most of the rim of the Canada Basin except for the short section to the west of Banks Island.

During the freezing process from the late summer into the early fall (20 September to 20 October), the ice cover remained off the continental shelf of the Chukchi and Beaufort Seas with only less than 10% of sea ice over bathymetry shallower than 500 m as seen in the (a) and (c) plots in Figure 4. Correspondingly, the isobaths that conformed most closely to the sea ice edges were at 2300 m and 1300 m deep as shown in panels (b) and (d) in Figure 4. Later in the fall (20 November 2009), sea ice cover grew and expanded to the northern Alaska coast while the boundary of seasonal ice still maintained its position around the shelf break conforming most closely with the isobaths at 1700 m deep (Figure 4f), and there was less than 3% of perennial ice over bathymetry shallower than 400 m (Figure 4e).

3.3. Barents and Greenland Seas

In the Barents Sea, complex water mass distributions are modified by mixing between Atlantic and Arctic waters (Pfirman et al., 1994; Harris et al., 1998). Bathymetry exerts a strong control on spatial patterns of the waters (Johannessen and Foster, 1978), which govern the location of the Barents Sea Polar Front (BSPF), which is the interface between warm Atlantic and cold Arctic water masses (Gawarkiewicz and Plueddemann, 1995).

From the IBCAO data, Figure 5 presents the complicated bathymetry in the Barents Sea where major features include the Bear Island Trough between the Svalbard Bank and Norway, the Franz Josef-Victoria Trough between Kong Karls Land and Franz Josef Land, and the Svyataya Anna Trough between Franz Josef Land and Novaya Zemlya, with the Great Bank and the Central Bank occupying the central region. Guided by these seafloor features are warm currents including the West Spitsbergen Current and the North Cape Current respectively in

western and southern regions, while cold-water inflows are from the north and the east through the Franz Josef-Victoria Trough and the Svyataya Anna Trough.

Warm and cold surface waters controlled by the seafloor features impact the formation and evolution of sea ice in the Barents Sea (Nghiem et al., 2005). In spring, extensive sea ice formation has typically expanded over the Svalbard Bank and the Great Bank and may advance farther south across the Central Bank. To observe springtime sea ice patterns in the Barents Sea, QS data are used to map sea ice on 3 April, about two weeks after the spring equinox, of each year in the decade of the 2000s (2000-2009). Two distinctive cases are discovered from the sea ice patterns: (1) Sea ice edges in the north of the Central Bank in years 2000, 2001, and 2005-2009 shown in Figure 6, and (2) sea ice edges over the Central Bank and extended farther south in years 2002-2004 presented in Figure 7.

In the first case (Figure 6), the sea ice edges are located on shallow bathymetry to the west and south of Svalbard. These ice edges advanced across the Great Bank, and remained to the north of the Central Bank. Despite large variability in atmospheric dynamics, temperature, and solar radiation conditions (depending on cloud covers) among those years in these cases (2000, 2001, and 2005-2009), all of the sea ice cover had a southern tip around Bear Island, recurrently covered the Svalbard Bank. The ice edges in those years remained close together along an extensive distance of 1500 km from the west of Svalbard, curving around the Svalbard Bank, and stretching along the deep channel separating the Great Bank to the north and the Central Bank to the south. Although the 2006 ice edge was offset to the north of this channel on 3 April, it was there just three days earlier before strong southeasterly winds forced its retreat. Farther to the east toward Novaya Zemlya, the bathymetry becomes more complex together with variable

water mixing from inflows of cold and warm currents, resulting in sea ice existing at different locations in different years.

In the second case (Figure 7), the ice edges were very different in different years (2002-2004) across the Barents Sea. In 2002 and 2004, the ice edges remained close to the southern tip of Svalbard and well to the north of the 2003 ice edge in the western region of the Beaufort Sea. In contrast, in the eastern region of the Barents Sea, the 2002 and 2004 ice covers were more extensive than that in 2003 off the southwest coast of Novaya Zemlya. Nevertheless, there exists a common feature in the 2002-2004 sea ice cover, which protruded southward across the Central Bank in the central region of the Barents Sea. The 2002 sea ice cover remained on the Central Bank whereas the south tip of the 2004 sea ice cover advanced beyond the Central Banks. The 2003 ice edge reached the southernmost, as far as 225 km away from the south end of the Central Bank. Changes in atmospheric and radiation forcing might contribute to the large differences in the locations of sea ice in 2002-2004. Nevertheless, the southward advance of ice edge across the Central Bank suggests a weaker supply of warm water from the south, a stronger supply of cold water from the north, or both.

Coincidentally, in the Greenland Sea, the Odden ice tongue (Figure 8) was extensive and well defined in 2003 and 2004, the years when the ice edges extended south beyond the Central Bank. The tip of the Odden ice tongue on 23 April 2003 (Figure 8a) was approximately 370 km from the closest break of the Greenland continental shelf, and that on 21 February 2004 (Figure 8b) was 470 km away from the shelf break and stretched beyond the Prime Meridian. These ice tongues curled around within the limit of the Jan Mayen fracture zone and the Mohns Ridge (Figure 8c). In the north of Jan Mayen fracture lie the Odden region and the Nordbukta region,

where seafloor features govern oceanic gyre, plumes, and currents and thus impact sea ice melting and freezing processes (Carsey and Garwood, 1993; Vinje et al., 2002).

While wind and temperature are among the important factors in the formation of Odden ice tongue, effects of bathymetry can be identified through the formation process of the ice tongue in February 2004 (Figure 9). Instead of initially stretching out from the main ice pack along the Greenland continental shelf, sea ice started to form within a small isolated area (Figure 9b) located above a deep seafloor region. This initial sea ice area was 150 km away from the main ice pack on the Greenland shelf. Actually, a similar isolated sea ice area appeared during the period of 25-29 January 2004, then it melted away (see Figure 9a for 2 February) and reappeared on 3 February 2004 (Figure 9b). The initial ice area grew larger and was still detached from the main sea ice pack (Figures 9b-d) until 10 February 2004 when it started to connect to the coastal ice pack (Figure 9e). By 14 February, the Odden ice tongue was well developed (Figure 9f). During this formation process, sea ice areas in all of the different growth stages were within the limit of the Jan Mayen fracture and the Mohns Ridge (Figure 9g). The early development of the Odden ice tongue from sea ice formed offshore and isolated from the coastal ice suggests the presence of cold waters associated with the cyclonic ocean circulation imposed by the bathymetry.

Regarding the main sea ice cover, it primarily occupied the Greenland continental shelf and the ice edge typically extends to around the yellow contour in Figure 9g. Such primary residence of sea ice on the Greenland shelf is confirmed with buoy tracks compiled over the past three decades since 1979 from the International Arctic Buoy Programme (http://iabp.apl.washington.edu/). Although a number of floatable buoys could drift across the deep ocean, tracks of 'ice' buoys (deployed on ice and sunk when ice melted) traced mostly over

the continental shelf in the Greenland Sea (Figure 10). Quantitatively, our analysis of the histogram of buoy positions as a function of water depth shows that only 27% of the buoys, including ice buoys and floatable buoys, were in water deeper than 1400 m between 70^{o}N and 80^{o}N in the Greenland Sea in the extensive time period from 1979 to 2010.

3.4. Across the Arctic Ocean

Beyond the local scale and regional extent that stretches over 1000 km, bathymetry control on sea ice cover can also be observed on the basin-scale across the Arctic Ocean. As an example, Figure 11 presents QS sea ice cover for 3 November 2007, less than two months after the record reduction of the total sea ice extent in September 2007. This observation shows the extensive conformation of the perennial sea ice boundary along the continental shelf breaks of the Greenland Sea, Barents Sea, Kara Sea, and Laptev Sea (Figure 11). Perennial ice occupied the shallow region of the Greenland continental shelf, spanned across the deep channel in the Fram Strait, and covered the deep basin off the shelves of the Barents, Kara, and Laptev Seas along the south side of the Nansen Basin. This perennial ice conformation is maintained over an extremely large distance of 3700 km across the Arctic Ocean. Seasonal ice that survives the summer melt preferentially on cold water regions, governed by bathymetry characteristics, seasonal sea ice becomes perennial ice by definition (Armstrong et al., 1973; Nghiem et al., 2006), resulting in such extensive conformation with the continental shelf breaks. The close match between the perennial ice boundary and the shelf bathymetry is presented in Figure 12, where the best-conformed isobath was at 1400 m along the Greenland sector and at 2300 m along the Nansen Basin south side.

4. Summary and Discussions

Bathymetry plays an important role in the formation and evolution of sea ice from local areas to extensive regions in the Arctic Ocean. In summary, we have found that:

1. In the Bering Sea, the maximum SIE reaches the shelf break in spring (case study in March 2008). Sea ice forms and remains over the shallow bathymetry on the continental shelf. The ice edge aligns with the shelf-break bathymetry spanning over 1200 km.

2. In the Chukchi and Beaufort Seas, the sea ice edge is close to the shelf break during the freeze-up transition from the summer to the fall season (case study in September to November 2009). In this case, sea ice preferentially remains over the deep bathymetry as opposed to the case of the Bering Sea. As the sea ice survives the summer melt and becomes perennial ice, the boundary of the perennial ice and other ice classes continues to conform to the vicinity of the shelf break across an extensive length of 1670 km.

3. In the Barents and Greenland seas, the bathymetry control on the sea ice cover is evident from sea ice maps during the decade of 2000s. For the Barents Sea, two distinctive cases are discovered from the sea ice patterns: Sea ice edges in the north of the Central Bank in years 2000, 2001, and 2005-2009, and sea ice edges over the Central Bank and extended further south in years 2002-2004. Additionally, in 2003 and 2004, the Odden ice tongue was extensive and well defined within the limit of Jan Mayen fracture zone and the

Mohns Ridge. Overall, sea ice resides preferentially over the continental shelf in the Greenland Sea.

4. Across the Arctic Ocean, perennial ice occupied the shallow region of the Greenland continental shelf, spanned across the deep channel in the Fram Strait, and covered the deep basin off the shelves of the Barents, Kara, and Laptev Seas. This conformation spans over an extensive distance of 3700 km across the Arctic Ocean.

From these results, there are several important implications. There are geological features that control and constrain the maximum SIE. Sea ice can grow and extend to the limit of the shoreline around the Arctic Ocean, the continental shelf break in the Bering Sea, over the continental shelf of the Greenland Sea, and the polar front in the Barents Sea that is governed by the regional bathymetry. Although there is some inter-annual variability, the maximum SIE in spring remains stable because of the geological influence, compared to the large reduction in the minimum SIE by the end of the summer melt in the last decade (Table 1).

The seafloor structures can dictate where perennial sea ice resides across the Arctic Ocean: over the deep basin off the continental shelf of the Laptev Sea, the Kara Sea, and Barents Sea, and over the continental shelf of the Beaufort Sea. This distribution of perennial sea ice is coincidentally located along the primary path of the Transpolar Drift. In strong Polar Express events driven by strong wind forcing supported the atmospheric dipole anomaly (Nghiem et al., 2007), an excessive transport of perennial sea ice out of the Arctic via the Fram Strait can results in massive ice loss since perennial ice is the older and thicker type of sea ice compared to first year or seasonal sea ice. While the Polar Express is driven by anomalous winds, the direction of

the ice transport along the Transpolar Drift is not arbitrary as it is limited in the deep transpolar basins such as the Nansen Basin, and aligned along Lomonosov Ridge across the Arctic Ocean (Alkire et al., 2007). Such bathymetry control on the location of perennial sea ice sets up a condition conducive to an abrupt reduction of perennial sea ice, which in turn preconditions the large decrease of the total SIE during summer.

In the Chukchi Sea and the Beaufort Sea, warm water on the continental shelf hinders the sea ice freeze-up process. Consequently, prolonged open water conditions allow more latent heat flux to form more cloud cover over the region. During diminished insolation conditions in the fall season, the blanket effects (Perovich et al., 1999) become dominant and long-wave radiation reflected back to the ocean can further delay the growth of sea ice. Since the water continues to stay warm, sea ice can be melt from the bottom in the late summer (Steele et al., 2009) and may not grow readily in the early fall. This process is a positive feedback that enhances thermodynamic effects in retarding the formation of sea ice cover over the continental shelf of the Chukchi Sea and Beaufort Sea.

Since the seafloor features are stable (on the geological time scale), the bathymetry control on sea ice patterns means that the ice growth and evolution processes can recur around certain geophysical structures on the seafloor in the Arctic Ocean. Such recurrence in sea ice patterns suggests the need to account for bathymetry effects in forecast and seasonal outlook models in order to achieve good predictability. Since the distribution of warm and cold waters governed by the bathymetry is a very slowly varying factor, short-term forecast and seasonal outlook of sea ice can have a higher level of confidence as compared to the forecast or outlook of other environmental parameters that are rapidly changing under rapidly-changing meteorological influences.

While this paper presents evidence of seafloor control on sea ice in various cases in the Bering, Chukchi, Beaufort, Barents, and Greenland seas and across the Arctic Ocean (from the Greenland Sea across the Barents Sea and Kara Sea to the Laptev Sea), the frequency of recurrence of these sea ice patterns needs to be investigated with decadal-scale datasets from multiple satellite sensors including synthetic aperture radar, scatterometer, microwave radiometer, and multi-spectral radiometer. Moreover, long-term measurements of atmospheric and oceanic parameters including surface temperature, pressure, and hydrographic observations are necessary to understand and explain the interactions that are influenced by the bathymetry that affect sea ice formation and evolution. Such understanding will provide further physical insights into the sea ice formation and evolution processes that can help improve our forecast, outlook, and projection models.

Acknowledgments

The research carried out at the Jet Propulsion Laboratory, California Institute of Technology, was supported by the National Aeronautics and Space Administration (NASA) Cryospheric Sciences Program. Rigor is funded by NASA, and the contributors to the International Arctic Buoy Programme (IABP), which include the International Arctic Research Center, NASA, NAVO, NIC, NOAA, NSF, ONR, and U.S. Coast Guard. The views, opinions, and findings contained in this report are those of the authors and should not be construed as an official National Oceanic and Atmospheric Administration, or any other U.S. government position, policy, or decision.

References

Ackerman, S.A., Holz, R.E., Frey, R., Eloranta, E.W., Maddux, B., McGill, M., 2008. Cloud detection with MODIS: Part II Validation, J. Tech., 25, 1073-1086.

Alkire, M.B., Falkner, K.K., Rigor, I., Steele, M., Morison, J., 2007. The return of Pacific waters to the upper layers of the central Arctic Ocean, Deep-Sea Res. Part I, 54, 1509−1529.

Allison, I.N., Bindoff, L., Bindschadler, R.A., Cox, P.M., de Noblet, N., England, M.H., Francis, J.E., Gruber, N., Haywood, A.M., Karoly, D. J., Kaser, G., Le Quéré, C., Lenton, T.M., Mann, M.E., McNeil, B.I., Pitman, A.J., Rahmstorf, S., Rignot, E., Schellnhuber, H.J., Schneider, S.H., Sherwood, S.C., Somerville, R.C.J., Steffen, K., Steig, E.J., Visbeck, M., Weaver, A.J., 2009. The Copenhagen Diagnosis, 2009: Updating the World on the Latest Climate Science. The University of New South Wales Climate Change Research Centre (CCRC), Sydney, Australia, 60 pp.

Armstrong, T., Roberts, B., Swithinbank, C., 1973. Illustrated Glossary of Snow and Ice, 2nd ed., Scott Polar Res. Inst., Cambridge, U. K.

Bourke, R.H., Paquette, R.G., Blythe, R.F., 1992. The Jan Mayan Current of the Greenland Sea, J. Geophys. Res., 97, C5, 7241−7250.

Carmack, E., Chapman, D.C., 2003. Wind-driven shelf/basin exchange on an Arctic shelf: The joint roles of ice cover extent and shelf-break bathymetry, Geophys. Res. Lett., 30, 14, 1778, doi:10.1029/2003GL017526.

Carsey, F.D., Garwood, R.W., 1993. Identification of modeled ocean plumes in Greenland gyre ERS-1 SAR data, Geophys. Res. Lett., 29(20), 2207-2210.

Comiso, C.C., Wadhams, P., Pedersen, L.T., Gersten, R.A., 2001. Seasonal and interannual variability of the Odden ice tongue and a study of environmental effects, J. Geophys. Res., 106, C5, 9093−9116.

Gawarkiewicz, G., Plueddemann, A. J., 1995. Topographic control of thermohaline frontal structure in the Barents Sea Polar Front on the south flank of Spitsbergen Bank, J. Geophys. Res., 100(C3), 4509-4524.

Harris, C.L., Plueddemann, A.J., Gawarkiewicz, G.G., 1998. Water mass distribution and polar front structure in the western Barents Sea, J. Geophys. Res., 103(C2), 2905-2917.

Jakobsson, M., Cherkis, N.Z., Woodward, J., Macnab, R., Coakley, B., 2000. New grid of Arctic bathymetry aids scientists and map makers, Eos Trans. AGU, 81, 9, pp. 89, 93, 96.

Jakobsson, M., Macnab, R., Mayer, L., Anderson, R., Edwards, M., Hatzky, J., Schenke, H.W., Johnson, P., 2008. An improved bathymetric portrayal of the Arctic Ocean: Implications for ocean modeling and geological, geophysical and oceanographic analyses, Geophysical Research Letters, doi:10.1029/2008GL033520.

Johannessen, O.M., Foster, L.A., 1978. A note on the topographically controlled oceanic polar front in the Barents Sea, J. Geophys. Res., 83(C9), 4567-4571.

Kalnay, E., Kanamitsu, M., Kistler, R., Collins, W., Deaven, D., Gandin, L., Iredell, M., Saha, S., White, G., Woollen, J., Zhu, Y., Leetmaa, A., Reynolds, R., Chelliah, M., Ebisuzaki, W., Higgins, W., Janowiak, J., Mo, K.C., Ropelewski, C., Wang, J., Jenne, R., Joseph, D., 1996. The NCEP/NCAR 40-year reanalysis project, Bull. Amer. Meteor. Soc. 77, 437-471.

Mahoney, A., Eicken, H., Gaylord, A.G., Shapiro, L., 2007. Alaska landfast sea ice: Links with bathymetry and atmospheric circulation, J. Geophys. Res., 112, C02001, doi: 10.1029/2006JC003559.

Martin, S., Drucker, R., 1997. The effect of possible Taylor columns on the summer ice retreat in the Chukchi Sea, J. Geophys. Res., 102, C5, 10473−10482.

National Geophysical Data Center, 1988. Data Announcement 88-MGG-02, Digital relief of the Surface of the Earth, NOAA, Boulder, Colorado.

Nghiem, S.V., 1998. Sea ice surface thermal states in polar regions, Submarine-based Arctic Science after the Year 2000, Warrenton, Virginia, available at Jet Propulsion Laboratory Tech. Report Serv. http://trs-new.jpl.nasa.gov/dspace/bitstream/2014/20498/1/98-1485.pdf

Nghiem, S.V., Van Woert, M.L., Neumann, G., 2005. Rapid formation of a sea ice barrier east of Svalbard, J. Geophys. Res., 110, doi:10.1029/2004JC002654.

Nghiem, S.V., Chao, Y., Neumann, G., Li, P., Perovich, D.K., Street, T., Clemente-Colón, P., 2006. Depletion of perennial sea ice in the East Arctic Ocean, *Geophys. Res. Lett.*, *33*, L17501, doi:10.1029/2006GL027198.

Nghiem, S.V., Neumann, G., 2007. Arctic Sea-Ice Monitoring, in: 2007 McGraw-Hill Yearbook of Science and Technology, pp. 12−15, McGraw-Hill, New York.

Nghiem, S.V., Rigor, I.G., Clemente-Colón, P., Perovich, D.K., Richter-Menge, J., Chao, Y., Neumann, G., Ortmeyer, M., 2008. Recent state of Arctic sea ice, Eos Trans. AGU, 89(53), Fall Meet. Suppl., Abst. C44A-01.

Nghiem, S.V., Neumann, G., Clemente-Colón, P., Rigor, I.G, Perovich, D.K., 2011. Arctic perennial sea ice crash of the 2000s and its impacts, Proc. BioNature, Venice/Mestre, Italy.

Perovich, D.K., Andreas, E.L., Curry, J.A., Eicken, H., Fairall, C.W., Grenfell, T.C., Guest, P.S., Intrieri, J., Kadko, D., Lindsay, R.W., McPhee, M.G., Morison, J., Moritz, R.E., Paulson, C.A., Pegau, W.S., Persson, P.O.G., Pinkel, R., Richter-Menge, J.A., Stanton, T., Stren, H., Sturm, M., Tucker III, W.B., Uttal, T., 1999. Year on ice gives climate insights, Eos, Trans., Amer. Geophys. Union, 80, 41, 481 and 485–486.

Perovich, D.K., Nghiem, S.V., Markus, T., Schweiger, A., 2007a. Seasonal evolution and interannual variability of the solar energy absorbed by the Arctic sea ice-ocean system, J. Geophys. Res., 112, C03005, doi:10.1029/2006JC003558.

Perovich, D.K., Light, B., Eicken, H., Jones, K.F., Runciman, K., Nghiem, S.V., 2007b. Increasing solar heating of the Arctic Ocean and adjacent seas, 1979–2005: Attribution and role in the ice-albedo feedback, Geophys. Res. Lett., 4, L19505, doi:10.1029/2007GL031480.

Pfirman, S.L., Bauch, D., Gammelsrød, T, 1994. The northern Barents Sea: Water mass distribution and modification, in The Polar Oceans and their Role in Shaping the Global Environment: The Nansen Centennial Volume, Geophys. Monogr. Ser., Vol. 85, edited by Johannessen, O., Muench, R.D., Overland, J.E., pp. 77-94, AGU, Washington, D.C.

Richardson, K., Steffen, W., Schellnhuber, H.J., Alcamo, J., Barker, T. Kammen, D.M., Leemans, R., Liverman, D., Munasinghe, M., Osman-Elasha, B., Stern, N., Wæver, O., 2009. Synthesis Report from Climate Change, Global Risks, Challenges, and Decisions, second ed., Copenhagen, Denmark.

Shuchman, R.A., Josberger, E.G, Russel, C.A., Fischer, K.W., Johannessen, O.M., Gloersen, P., 1998. Greenland Sea Odden sea ice feature: Intra-annual and interannual variability, J. Geophys. Res., 103, C6, 12709−12724.

Stabeno, P.J., Reed, R.K., 1994. Circulation in the Bering Sea basin observed by satellite-tracked drifters: 1986-1993, J. Phys. Oceanogr., 24, 848−854.

Steele, M., Zhang, J., Ermold, W., 2010. Mechanisms of summertime upper Arctic Ocean warming and the effect on sea ice melt, J. Geophys. Res., 115, C11004, doi:10.1029/2009JC005849.

Stroeve, J., Holland, M.M., Meier, W., Scambos, T., Serreze, M., 2007. Arctic sea ice decline: Faster than forecast, Geophys. Res. Lett., 34, L09501, doi:10.1029/2007/GL029703.

Sturm, M., Perovich, D.K., Serreze, M.C., 2003. Meltdown in the North, Sci. Amer., 289,4, 60−67.

Tsai, W.-Y., Nghiem, S.V., Huddleston, J.N., Spencer, M.W., Stiles, B.W., West, R.D., 2000. Polarimetric scatterometry: A promising technique for improving ocean surface wind measurements, IEEE Trans. Geosci. Remote Sens., 38, 1903−1921.

Vinje, T., Løyning, T.B., Polyakov, I., 2002. Effects of melting and freezing in the Greenland sea, Geophys. Res. Lett., 29(23),2129, doi:10.1029/2002GL015326.

Woodgate, R., Weingartner, T., Lindsay, R., 2010. The 2007 Bering Strait oceanic heat flux and anomalous Arctic sea-ice retreat, Geophys. Res. Lett., 37, L01602, doi:10.1029/2009GL041621.

List of Figures

Figure 1. Sea ice cover (green-orange color scale) overlain on ETOPO5 bathymetry (in blue shades) in the Bring Sea, and annotation of ocean currents including the Alaskan Stream, Aleutian North Slope, Anadyr, and Kamchatka Currents.

Figure 2. Cumulative percentage of sea ice cover as a function of water depth in meters. The inset is a QS map of sea ice, including mixed ice, seasonal ice, and open water in different shades of blue from light to dark blue, respectively. The sea ice edge is in red and the best-conformed isobaths of 1300 m is in yellow. White areas are not considered in the analysis to determine the best-conformed isobaths.

Figure 3. Sea ice distribution in the Beaufort Sea on (a) 20 September 2009 with the yellow curve at the southern edge of the sea ice cover, (b) 20 October 2009 with the green curve at the southern edge of the sea ice cover, and (c) 20 November 2009 with the aqua curve at the southern edge between seasonal ice and other ice classes (perennial and mixed ice). The maps of sea ice classes are translucently overlain on the IBCAO bathymetry map which is presented separately without sea ice on panel (d) where the color scale represents water depth in meters.

Figure 4. Histogram of sea ice distribution and best-conformed isobaths for (a-b) 20 September 2009, (c-d) 20 October 2009, and (e-f) 20 November 2009. The left panels are for cumulative percentage of sea ice versus water depth. The right panels show the best conformed isobaths (yellow contour at depth indicated in yellow label in each panel) to the ice edges (red contour) in

panels (b) and (d), and to the seasonal ice boundary in panel (f), where open water, seasonal ice, mixed ice, and perennial ice are indicated with shades of blue from the darkest to the lightest, respectively. White areas are not considered in the analysis to determine the best-conformed isobaths.

Figure 5. Atlantic (red) and Arctic (white) waters across the Barents Sea overlain on a three-dimensional map of bathymetry from IBCAO data, after Nghiem et al. (2005).

Figure 6. Extents of sea ice cover across the Barents Sea on 3 April in seven years (2000, 2001, 2005-2009). The sea ice extent for each year is marked with a different color contour line. The background map represents IBCAO bathymetry with a blue-shade color key.

Figure 7. Extents of sea ice cover across the Barents Sea on 3 April in 2002-2004. The sea ice extent for each year is marked with a different color contour line. The background map represents IBCAO bathymetry with a blue-shade color key.

Figure 8. Extents of sea ice cover across the Greenland Sea on (a) 23 April 2003 delineated with the green contour line, and (b) 21 February 2004 delineated with the yellow contour line. In panels (a) and (b), red is for perennial sea ice, dark cyan for seasonal ice, light cyan for mixed ice, red for surface melt on sea ice, blue for open water, brown for land, and vertical blue line for 0^{o} longitude. IBCAO bathymetry map is shown in panel (c) together with the contour liness of sea ice edges.

Figure 9. Sea ice cover across the Greenland Sea on: (a) 2 February 2004, (2) 3 February 2004, (c) 4 February 2004, (d) 6 February 2004, (e) 10 February 2004, and (f) 14 February 2004. In panels (a)-(f), red is perennial sea ice, dark cyan is seasonal ice, light cyan is mixed ice, red is surface melt on sea ice, blue is open water, brown is land, and the vertical blue line is 0^o longitude. The IBCAO bathymetry map is shown in panel (g) together with the contours of sea ice edges having the same colors corresponding to different days in February 2004, where coastal Greenland sea ice edges are not drawn for days 3-10.

Figure 10. Buoy tracks (light gray dotted lines) in the Greenland Sea in three decades from 1979 to 2010, compiled with buoy location data from the International Arctic Buoy Programme. The thick yellow contour line corresponds most closely with the 1400-m isobath and the boundary of perennial sea ice is marked with the thick red contour line, corresponding to those in Figure 12. Thin yellow contour liness are represent other isobaths at different water depths.

Figure 11. Panel (a) presents sea ice cover across the Arctic Ocean on 3 November 2007, where red is perennial sea ice, dark cyan is seasonal ice, light cyan is mixed ice, red is surface melt on sea ice, blue is open water, brown is land, and the half circle in black is the North Pole area. Panel (b) shows the green contour line of the boundary between perennial sea ice and other types, which is overlain on the IBCAO bathymetry map. The contour of the perennial sea ice boundary is also plotted in Panel (a).

Figure 12. The isobaths (thick yellow contour lines) that conform most closely to the boundary of perennial sea ice (thick red contour) on a QS sea ice map on 3 November 2007, where open

water, seasonal ice, mixed ice, and perennial ice are indicated with shades of blue from the darkest to the lightest, respectively. The best-conformed isobath along the Greenland shelf break is at a depth of 1400 m, and that along the rise of the Nansen Basin is at a depth of 2300 m.

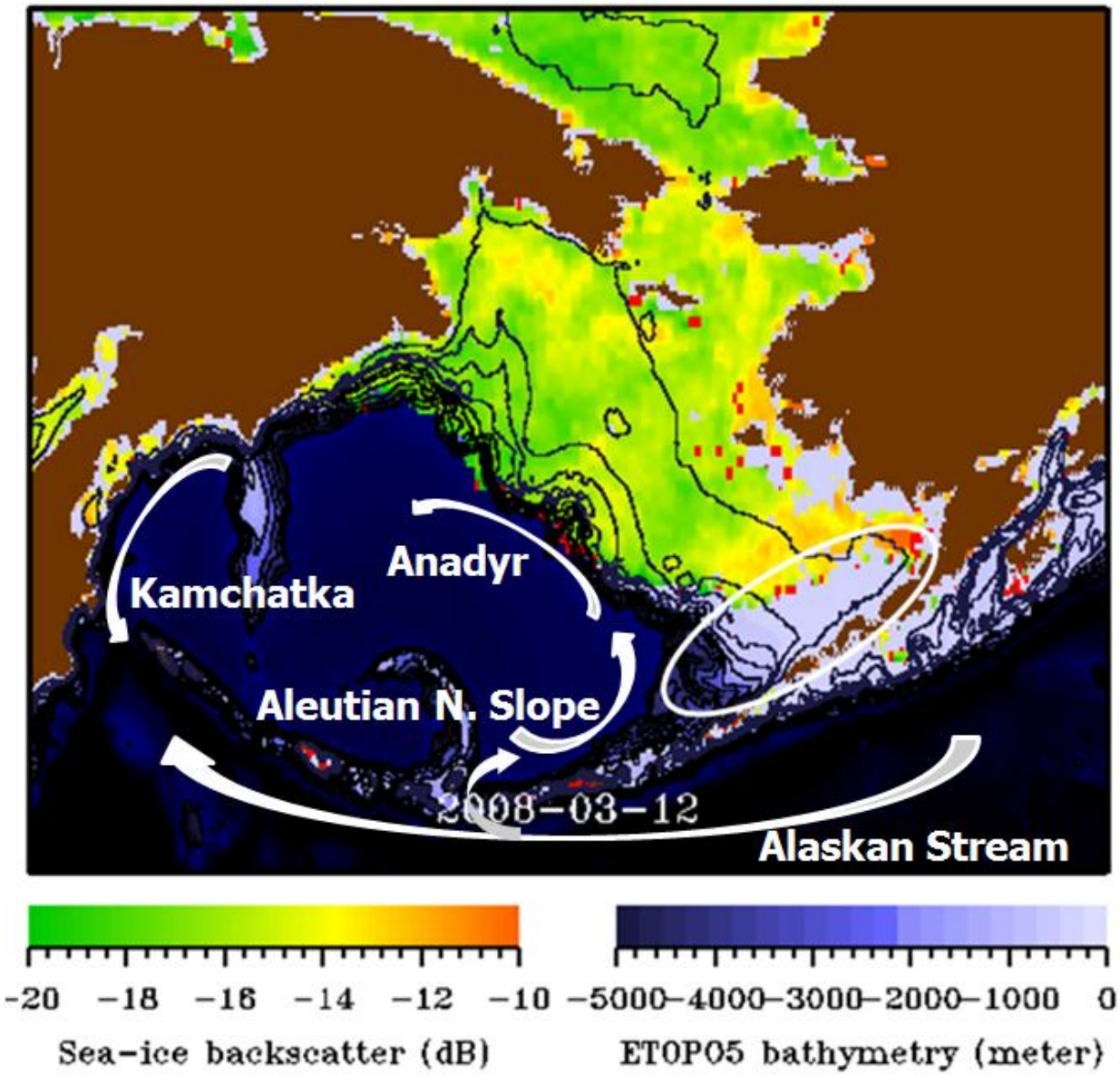

Figure 1.

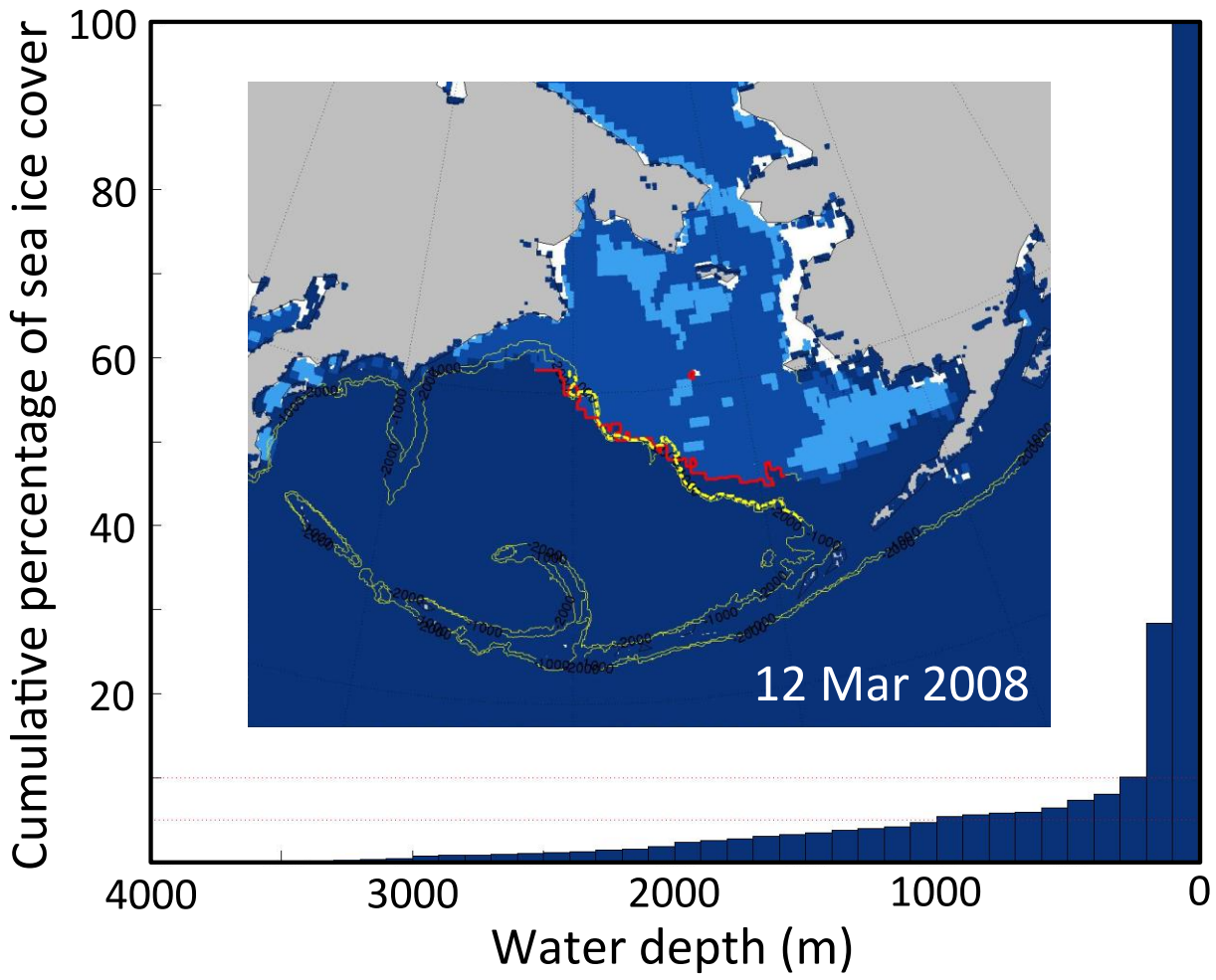

Figure 2.

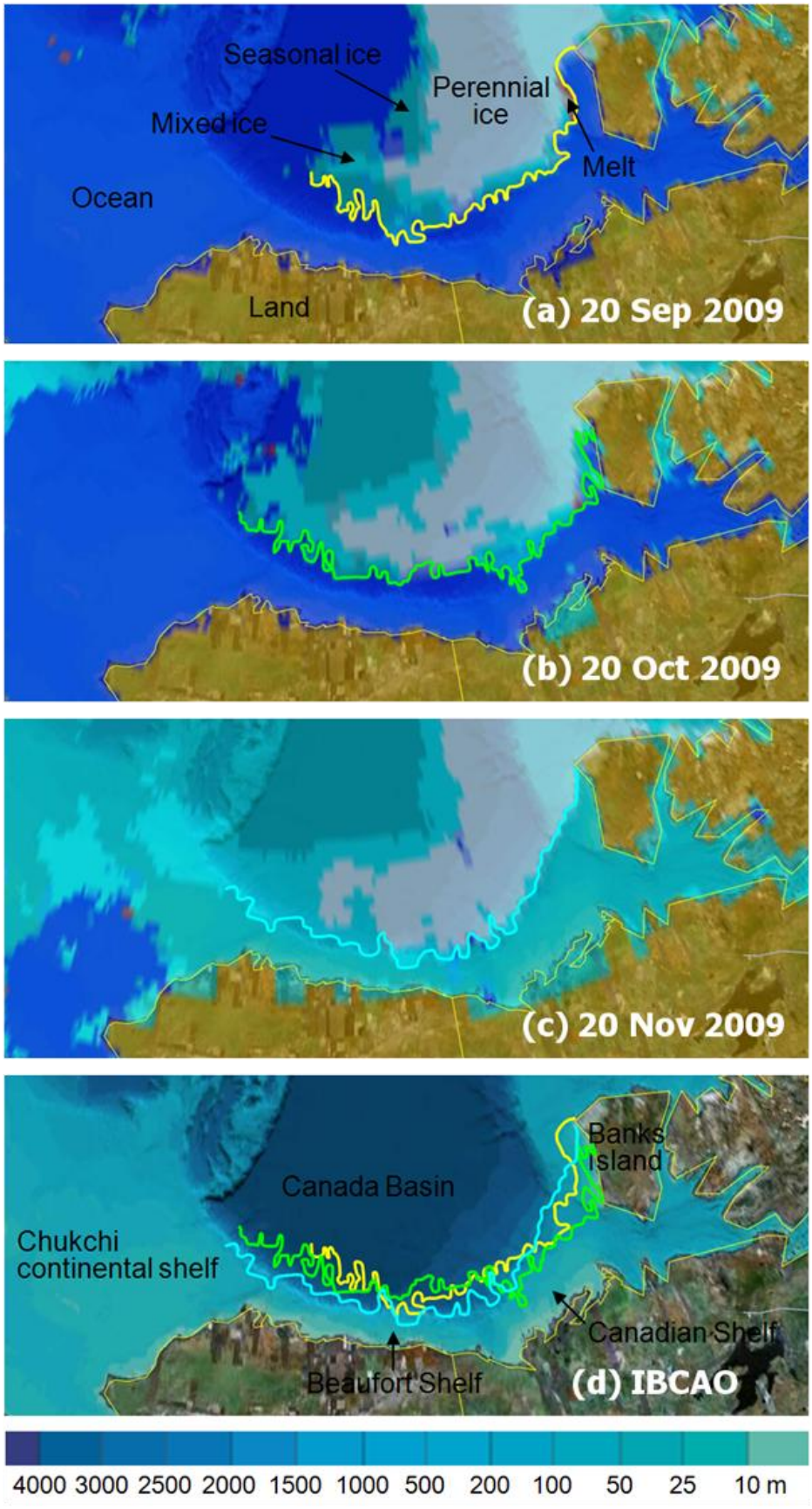

Figure 3.

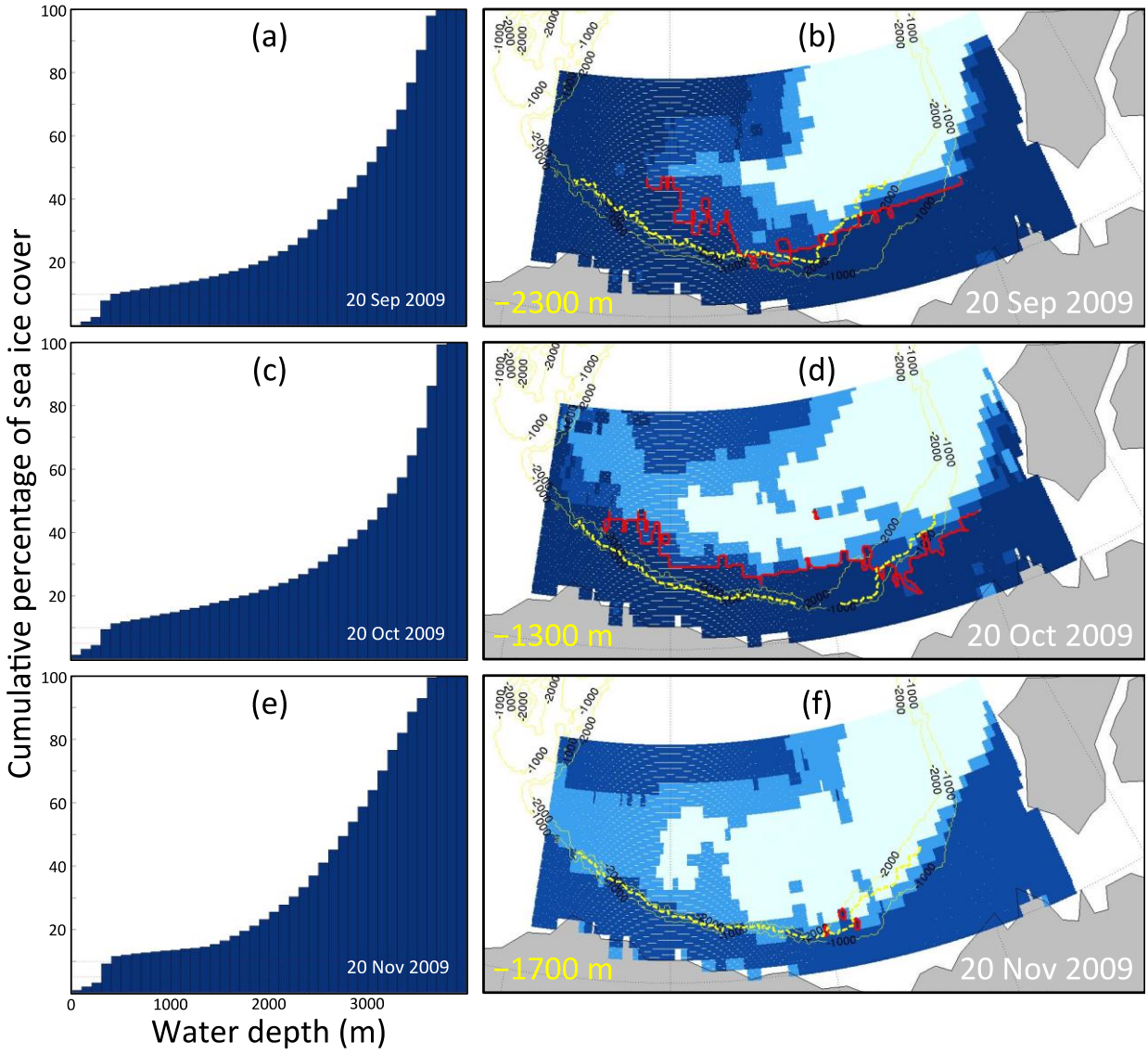

Figure 4.

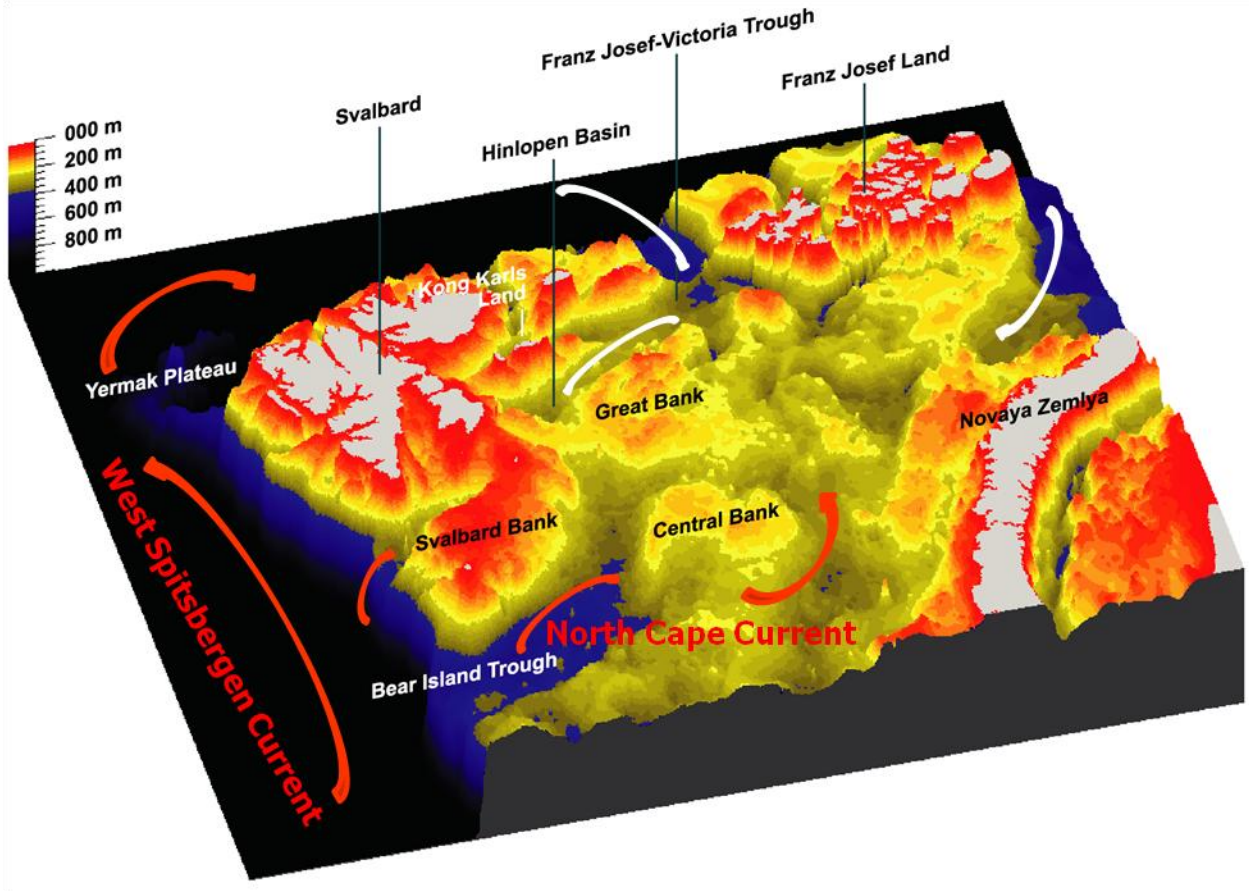

Figure 5.

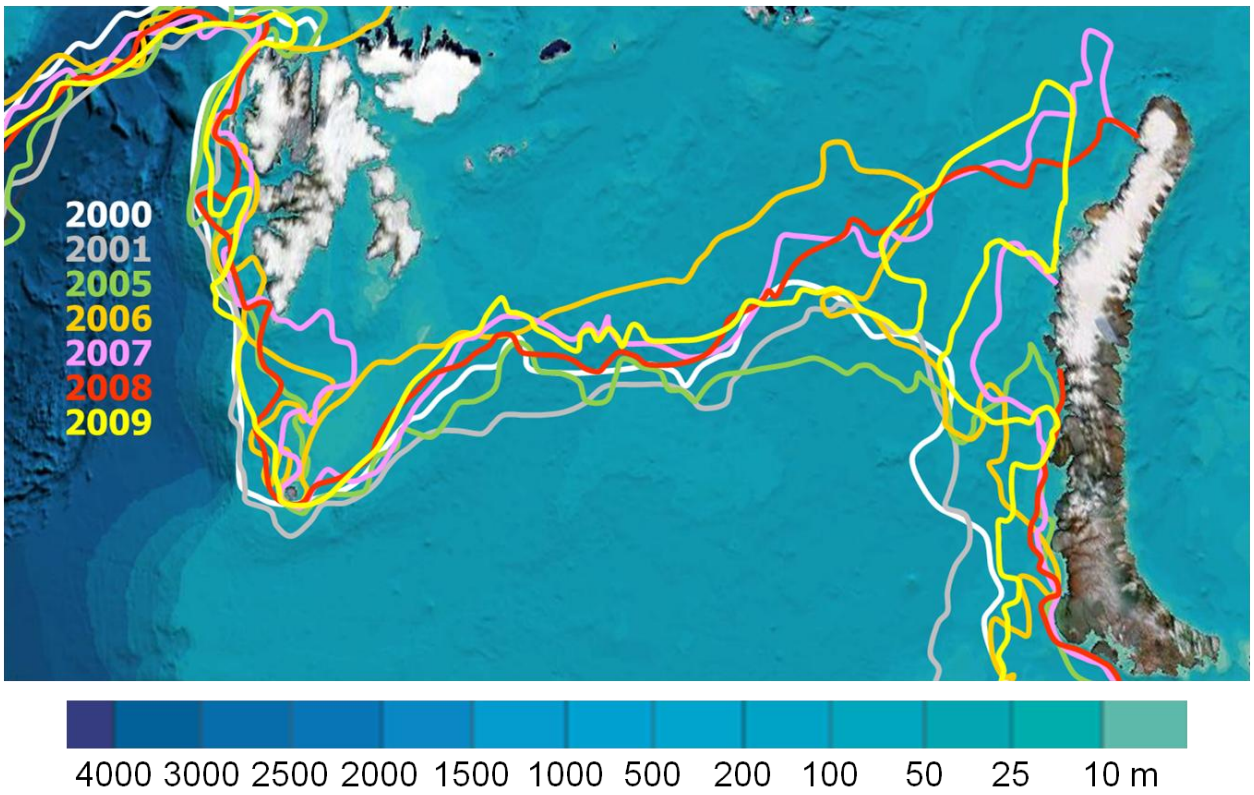

Figure 6.

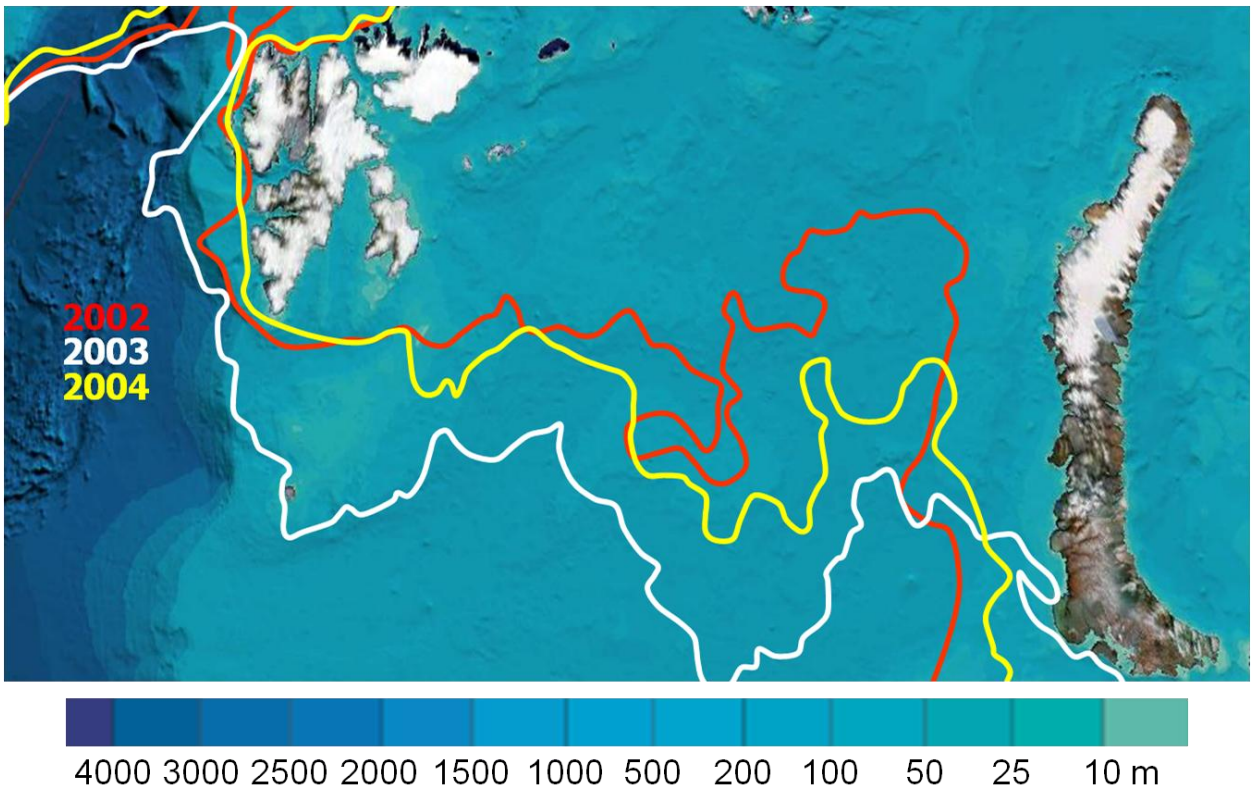

Figure 7.

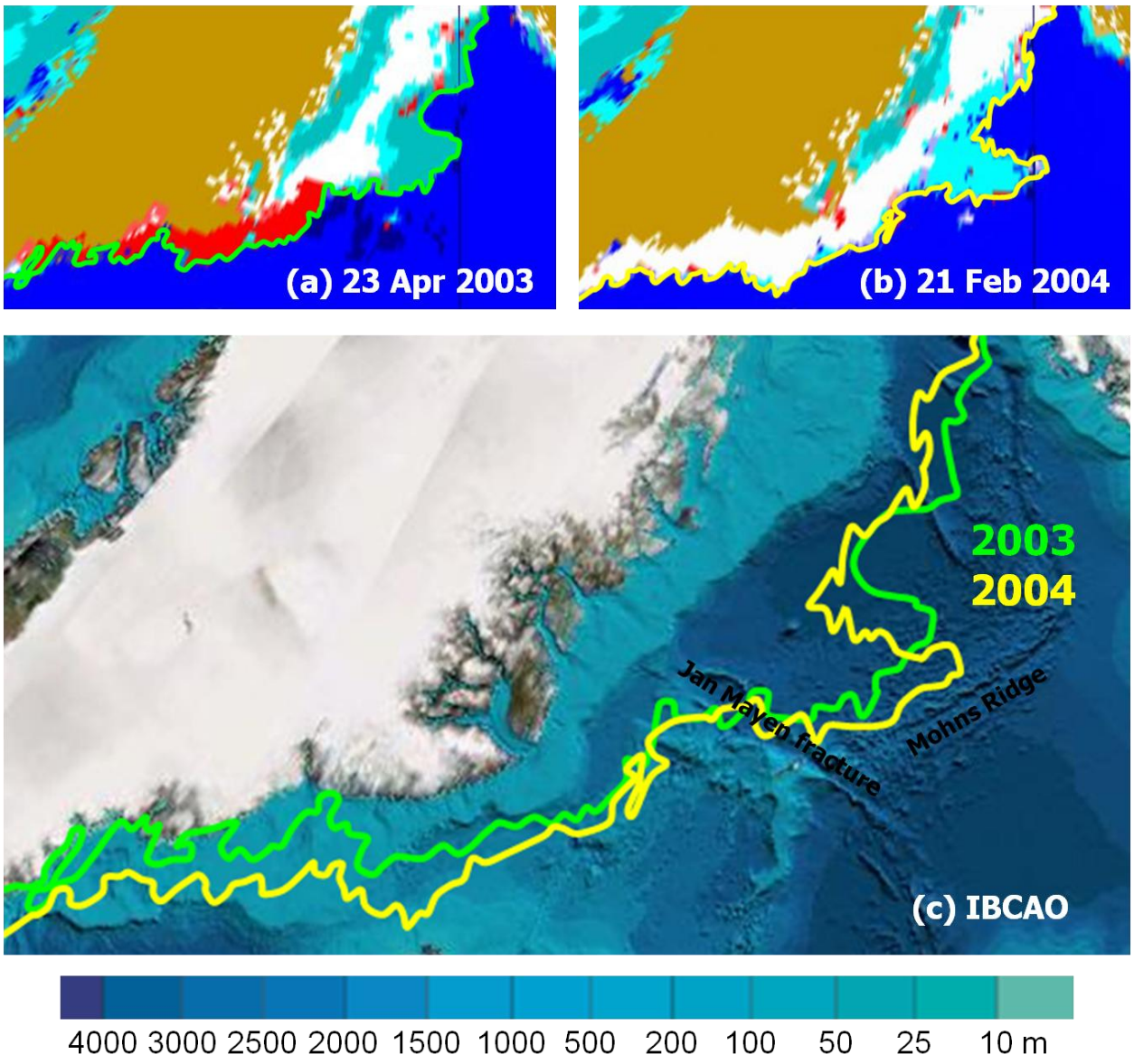

Figure 8.

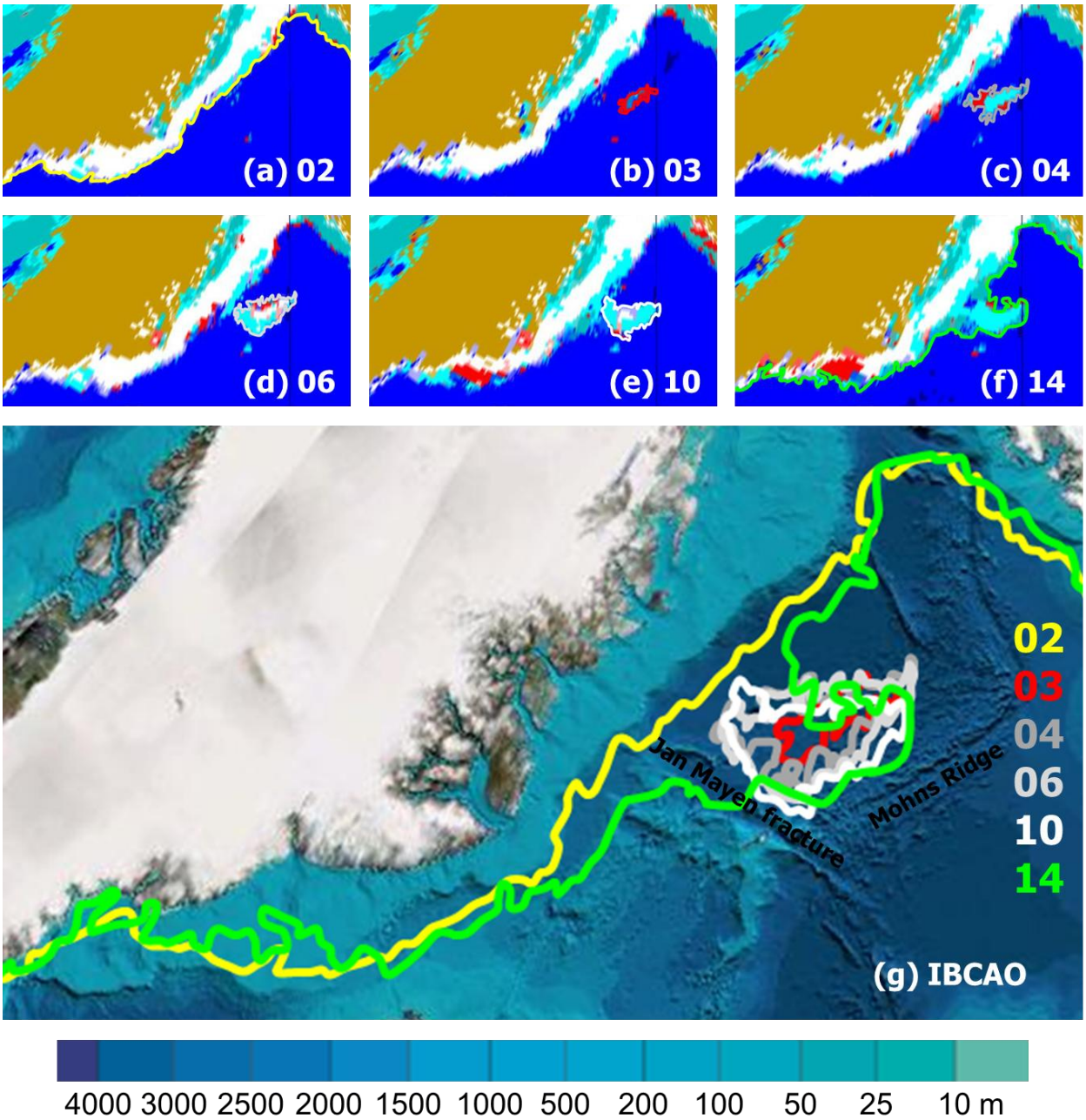

Figure 9.

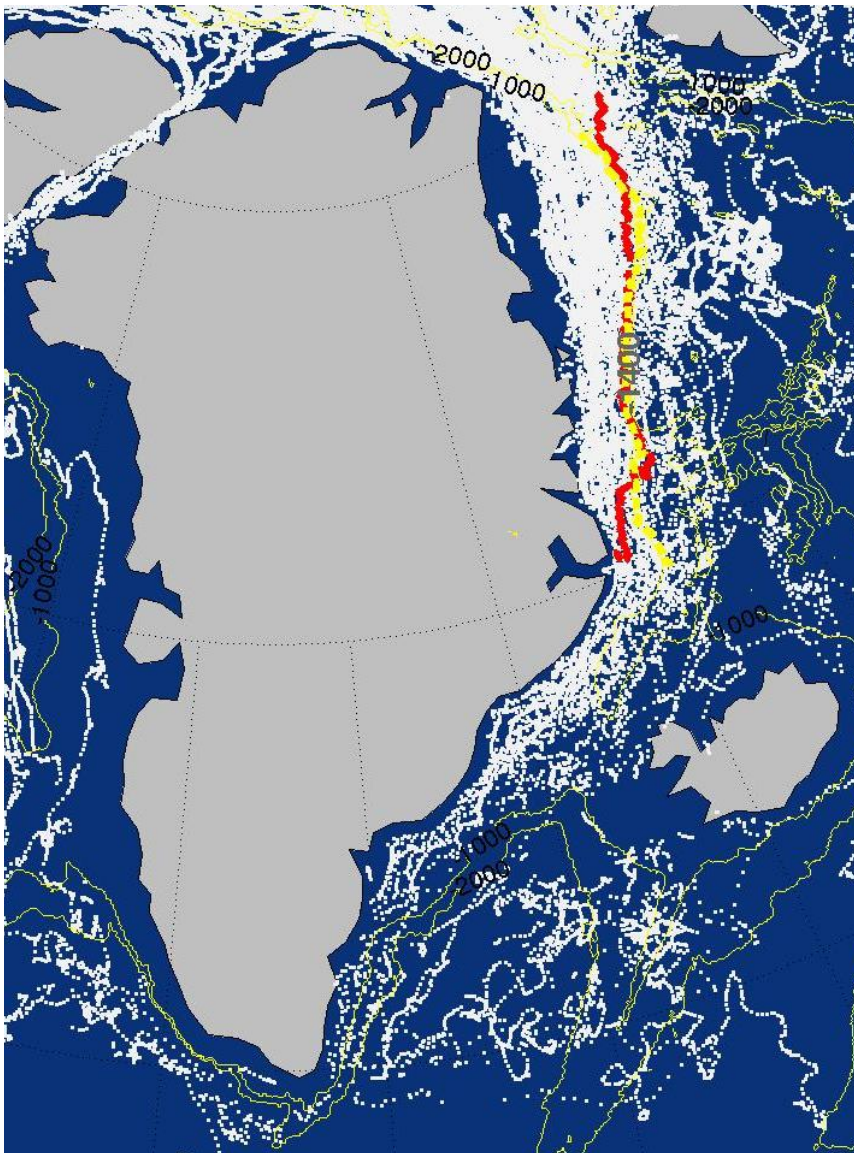

Figure 10.

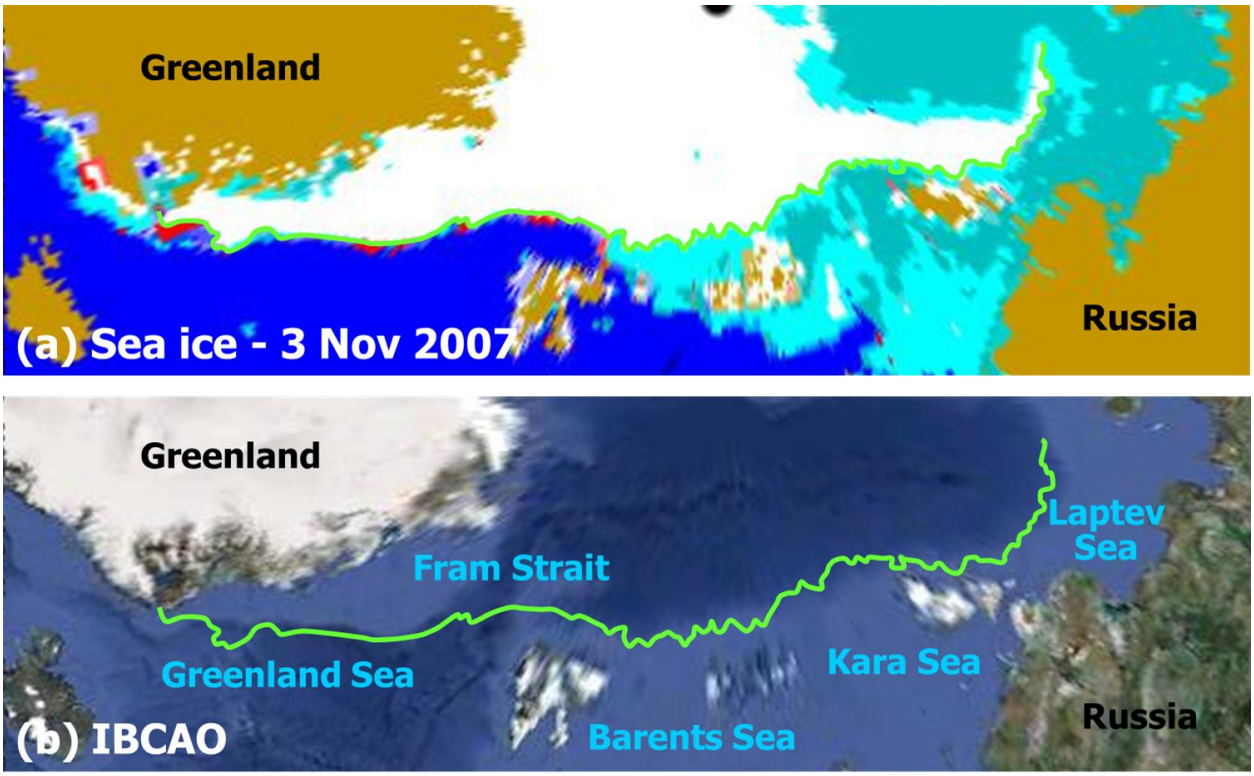

Figure 11.

Figure 12.

